Research on Control and Planning of Soft-Wing UAV for Haze Removal

Wei Huang, Liying Yang, Yuqing He, Bingbing Li

***Abstract*—The existence of fog and haze has caused great pollution to the environment. The research of removing haze is a hot topic in recent years. In this paper, a special haze removal algorithm based on Soft-Wing UAV is proposed. In this algorithm, two track control strategies are designed based on the Soft-Wing UAV model transfer function. A SIMULINK platform based mathematical model of Soft-Wing UAV is built to testified effectiveness of the two track control strategies. An autonomous ergodic-planning algorithm with greedy strategy and foldback algorithm for Soft-Wing UAV is designed. Within the algorithm, the haze regional has been modelled, the cost matrix is constructed, and the planning and ergodic strategy is proposed. Finally, the experimental results validates the reliability of the algorithm in the application of haze removal with the proposed evaluation Index.**

***Key words*—Soft-Wing UAV; Haze removal; Control strategies; Ergodic-planning algorithm.**

I. INTRODUCTION

Due to the requirement of industrial and economic development, the use of fossil fuels and the emission of harmful substances and soot aggravate the environmental pollution. Haze has become a frequent visitor to some cities in China in a short period. Haze has no longer simply referred to a weather state, but has become a natural disaster that affects human life[1]. In 2015, the WHO's International Cancer Research Institute issued a report for the first time to identify the carcinogenesis of air pollutants and consider it as a common and major environmental carcinogen[2]. In addition to the impact of human health, haze will also have a serious impact on the growth of plants and crops. When the pollutant reaches a certain concentration, it will cause the damage of plant physiological structure and eventually lead to plant wilt and death[3].

Manuscript received May 12, 2018. This work is supported by National Natural Science Foundation (NNSF) of China (Grant No.61503369) and Guangdong Province Science Foundation (Grant No.61503369).

Wei Huang is with the State Key Laboratory of Robotics, Shenyang Institute of Automation, Chinese Academy of Sciences, Shenyang 110016, Control Engineering, Northeastern University, Shenyang 110819, China (e-mail: 229669968@qq.com)

Liying Yang ,Yuqing He are with the State Key Laboratory of Robotics, Shenyang Institute of Automation, Chinese Academy of Sciences, Shenyang 110016, China (e-mails: {heyuqing, yangliying}@sia.cn).

Bingbing Li is with the State Key Laboratory of Robotics, Shenyang Institute of Automation, Chinese Academy of Sciences, Shenyang 110016, China (e-mails: libingbing@sia.cn).

In view of this grim situation, some haze removal methods emerge, as the times require. vehicles equipped with a mist canon can spray water mist up to 100 meters, in a bid to devour the smog, which can reduce the concentration of PM_2.5 in the air by 15% to 20%[4], but this method can not play a good role in the treatment of haze in a large and long time . Chen Yu[5] has designed a fog and haze intelligent helmet, which uses a lot of energy in the tail gas of the motorcycle to provide the energy for the equipment by cutting the magnetic line. It is both environmentally friendly and beneficial to the health of the motorcyclists. However, the fog and haze smart helmet can only be used with motorcycles. Meng et al[6], using electrostatic adsorption principle and electrostatic induction phenomenon, designed the electrostatic water curtain removing haze machine, which can make the haze dust removal efficiency up to 80%, but in practice, it does not have the conditions for application. Besides the methods mentioned, there are some other ideas to improve the quality of air[7-8], but need to be improved.

Soft-Wing unmanned aerial vehicle (UAV) is a new type of UAV, which is composed of an unmanned vehicle with a power device suspended through a rope. It has a simple structure, low cost and a big load weight ratio[9-11]. It is very suitable for long time air search and the automatic delivery of materials after the disaster. Soft wing UAV has low requirements for take-off and landing sites, short take-off distance, and a variety of simple takeoff methods [12-15]. It has the characteristics of independent take-off and landing, independent operation at high altitude and low cost [16-18]. Compared with the traditional quadrotor UAV flight control methods[19-22], control strategies for Soft-Wing UAV are easy to achieve and the control methods are simpler. Therefore, a method of haze removal using Soft-Wing UAV is proposed in this paper.

This paper first introduces the transfer function of five channels of the soft winged UAV identified by Li et al[23], then proposes two control strategies. The simulation of track point verifies the correctness of the control strategy. Then an improved greedy algorithm based on the cost function is proposed to realize the autonomous ergodicity planning. Finally, the haze simulation area is established, the simulation show the reliability of the proposed algorithm in the application of haze removal.

II. CONTROL AND PLANNING METHOD OF SOFT-WING UAV

A. *Model and control of soft-wing UAV*

Fig.1 Soft-Wing UAV Schematic Diagram

The soft wing UAV can be simplified as a black box model with four inputs and three outputs, and the transfer function model[23] of five channels can be obtained through parameter identification.

The input δ is the single-side pull-down distance, the output w is yaw angular velocity, and the transfer function model is shown in (1):

$$\frac{\Delta w(s)}{\Delta \delta(s)} = \frac{1.59\times10^{-4}s^2 + 8.19\times10^{-5}\text{s-}1.86\times10^{-5}}{s^4 + 0.569s^3 + 1.32s^2 + 0.437s + 0.9751} \quad (1)$$

The input S is the two-side pull-down distance, the outputs are forward velocity u and vertical velocity v, and the transfer function models are shown in (2) and (3).

$$\frac{\Delta u(s)}{\Delta S(s)} = \frac{-5.36\times10^{-3}s^3 - 1.01\times10^{-3}s^2 - 1.06\times10^{-3}s - 2.34\times10^{-3}}{s^4 + 1.236s^3 + 2.149s^2 + 1.54s + 0.164} \quad (2)$$

$$\frac{\Delta v(s)}{\Delta S(s)} = \frac{-2.36\times10^{-3}s - 3.01\times10^{-3}}{s^4 + 1.247s^3 + 2.132s^2 + 1.53s + 0.158} \quad (3)$$

The input T is engine throttle, the outputs are forward velocity u and vertical velocity v, and the transfer function models are shown in (4) and (5).

$$\frac{\Delta u(s)}{\Delta T(s)} = \frac{1.67\times10^{-3}s + 1.14\times10^{-3}}{s^4 + 1.252s^3 + 2.141s^2 + 1.535s + 0.168} \quad (4)$$

$$\frac{\Delta w(s)}{\Delta T(s)} = \frac{3.05\times10^{-3}s^2 + 2.14\times10^{-3}s - 1.04\times10^{-3}}{s^4 + 1.271s^3 + 2.153s^2 + 1.56s + 0.157} \quad (5)$$

The model simulation platform is built in SIMULINK shown in Fig.2.

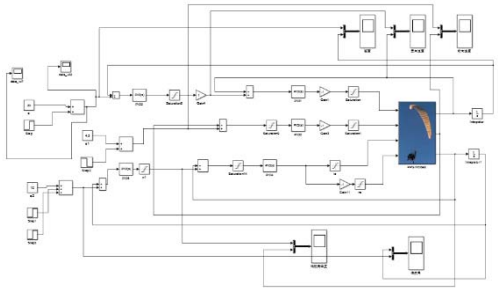

Fig.2 Simulation Diagram of Control algorithm

In order to verify the reliability and correctness of the simulation platform, the control simulation including forward velocity, vertical velocity and yaw angular velocity is carried out.

In the forward velocity control simulation, the initial state of the Soft-Wing UAV is the equilibrium point, and the forward velocity u is 5 m/s. As shown in Fig.3, at the 50th second, the expected value of the given forward velocity u is 4.2 m/s, the blue curve is the actual response curve of the forward velocity, and the red curve is the expected forward velocity response curve. At the 80th second, the forward velocity u reaches the expected value, the response time is 30 seconds, there is no overshoot. The control requirements are satisfied.

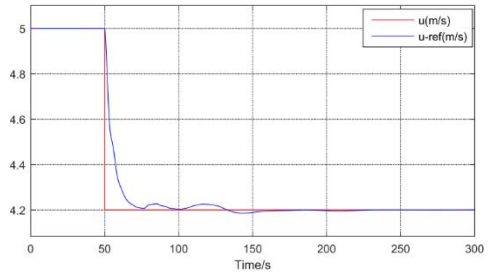

Fig.3 Forward velocity control curve

In the vertical velocity control simulation, the initial state of the Soft-Wing UAV is the equilibrium point, and the vertical velocity v is 0 m/s. As shown in Fig.4, at the 50th second, the expected value for a given vertical velocity v is -1 m/s. The blue curve is the actual response curve of the vertical velocity, and the red curve is the expected response curve of the vertical velocity. At the 100th second, the vertical velocity v reaches the expected value, the response time is 50 seconds, and the overshoot is 3.12%. The control requirements are satisfied.

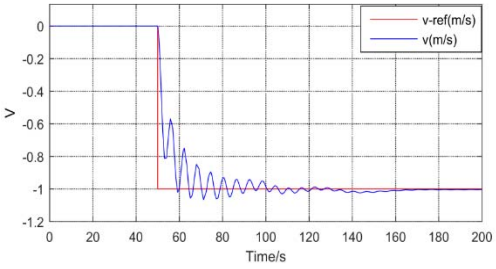

Fig.4 Vertical velocity control curve

In the simulation of yaw angular velocity control, the initial state of the Soft-Wing UAV is equilibrium point, and the yaw angular velocity w is 0 rad/s. The blue curve is the actual response curve of the yaw angular velocity, and the red curve is the expected response curve of the yaw angular velocity. As shown in Fig.5, at the 50th second, the expected value for a given yaw angular velocity w is -0.1 rad/s. At the 70th second, the yaw angular velocity w reaches the expected value, the response time is 20 seconds, and there is no overshoot. The control requirements are satisfied.

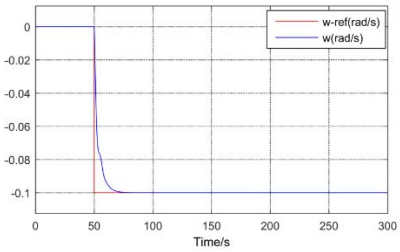

Fig.5 Yaw Angular velocity control curve

The simulation results show that the Soft-Wing UAV simulation platform based on the six-channel model can control forward velocity u, vertical velocity v,yaw angular velocity w. There is small overshoot and short response time. the control requirements are satisfied, verified the correctness of the model.

B. Track control of soft wing UAV

In the navigation trajectory control, there are two mainly control strategies: straight-to-line and turning.

The gradation of straight-to-line is shown in Fig.6. P is the current point position, A is the expected terminal point, M is the expected point at the previous moment, and T is the current point. The coordinates and path angle of the expected target point C at the next moment are:

$$psi = \tan(\mathrm{Ay}-\mathrm{My}, \mathrm{Ax}-\mathrm{Mx}) \tag{6}$$

$$C_x = T_x + (\|AT\| - \mathrm{R}) * \cos(\mathrm{psi}) \tag{7}$$

$$C_y = T_y + (\|AT\| - \mathrm{R}) * \sin(\mathrm{psi}) \tag{8}$$

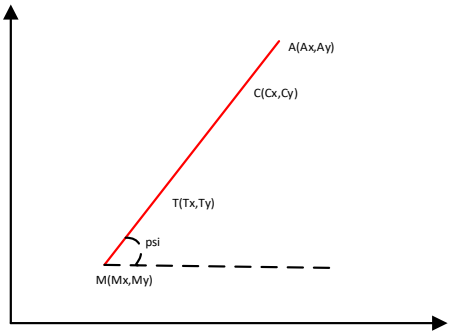

Fig.6 Diagrammatic sketch of straight-to-line

The gradation of turning is shown in Fig.7. P is the current point position, A is the expected terminal point, M is the expected point at the previous moment, and h is the vertical distance from the current point to the target line MA:

$$\mathrm{h} = \frac{-(A-M)\times(P-A)}{\|A-M\|} \tag{9}$$

Where:

$$t_1 = \frac{h}{v_h} = \frac{h}{v\sin(psi - psi^*)} \tag{10}$$

$$t_2 = \frac{psi - psi^*}{w} \tag{11}$$

since $t_1 = t_2$, the yaw angular velocity w can be solved.

$$\mathrm{w} = \frac{v * \sin(psi - psi^*) * (psi - psi^*)}{h} \tag{12}$$

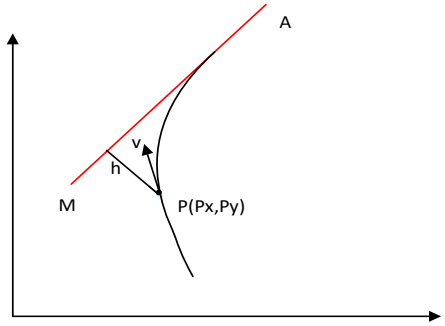

Fig.7 Diagrammatic sketch of straight-to-line

Based on the two control strategies of straight-to-line and turning, the Soft-Wing UAV flew at the track point as shown in Fig.8. The blue curve is the actual response curve of the yaw angular velocity, and the red curve is the expected response curve of the yaw angular velocity. The initial state point is (200,200,0), the initial yaw angle is 120 degrees, the initial advance distance is 200m. When the expected position point is reached, the Soft-Wing UAV flies to 50m altitude, then maintains the altitude and flies at the track finding point in turn. Fig.9 to Fig.11 show the state changes of forward velocity u, yaw angle ψ and altitude H, respectively. In the whole tracking process, comparing with the reference value (the red curve), forward velocity u, yaw angle ψ and flight altitude H can be controlled with short response time and small overshoot, which meets the basic requirements of flight controller. Through the track point simulation, the correctness of the two control strategies of straight-to-line and turning is verified, which further shows that the proposed control algorithm can meet the requirements of autonomous flight control of Soft-Wing UAV and provides a practical reference for the autonomous flight control algorithm of Soft-Wing UAV.

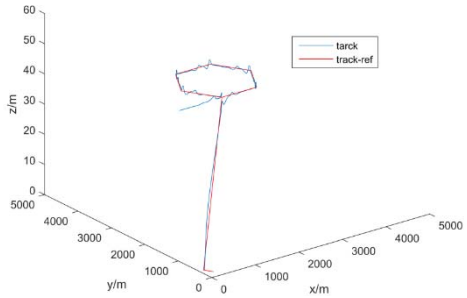

Fig.8 Trajectory tracking Curve of Soft-Wing UAV

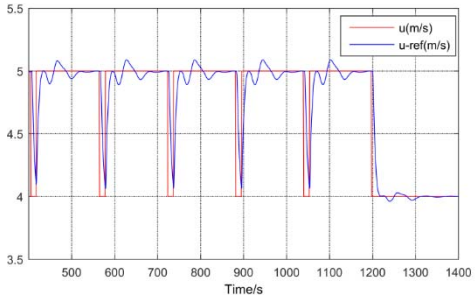

Fig.9 Forward velocity tracking curve

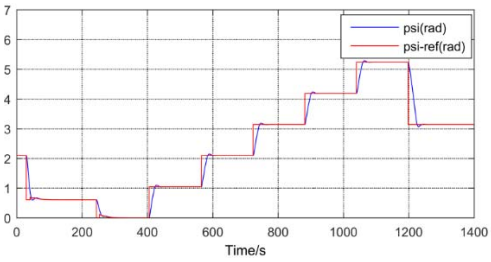

Fig.10 Yaw Angle tracking curve

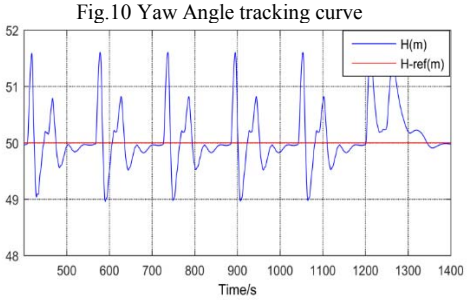

Fig.11 Height tracking curve

III. HAZE REMOVAL METHOD OF SOFT-WING UAV BASED ON GREEDY ALGORITHM

Soft-wing UAV works at high altitudes and often remain the altitude unchanged, so the ergodic area can be reduced to a two-dimensional plane. In this part, the haze region is divided firstly. Then the ergodic order of boundary points is determined. At last, an example is given to verify the foldback algorithm based planning and ergodic strategy is introduced.

A. *Region Division*

The ergodic region is assumed to be a rectangular area of $(4000\times1000)\,m^2$. The obstacles are assumed to be standard rectangles. Taking longitudinal division based on the position of obstacles, and the ergodic region can be divided into feasible sub-regions and obstacle regions.

In this paper, the ergodic region is divided into several sub-regions firstly. As shown in Fig.12, the red curve represents the boundary of the sub-regions. Then, the intersection points of sub-region need to be marked.

The first sub-region from left to right takes the center point of the left boundary marked A_1 as the first point, The last sub-region from left to right takes the center point of the right boundary marked as the last point, and the neighboring regions take the center point of the region intersection. As shown in Fig.12, $A_i\,(i=1\sim15)$ represents the chosen point.

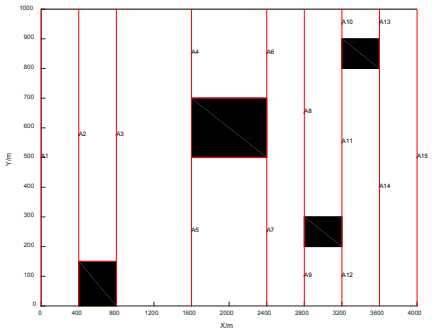

Fig.12 Regional Division and Points Taking Map

B. *Computation of the Cost Matrix*

After regions division, all feasible sub-regions needs to determine the ergodic order. This is an typical traveling salesman problem. In this paper, greedy strategy is used to solve the conventional problem. The order of path points is shown in Fig.13.

In the solving process, there are 2 rules must be obeyed. The first one is that for each sub-region, the left boundary point must connect to the right boundary point, which can ensure each sub-region be covered. For example, in Fig.13, the point order solved by greed strategy is *A1→A2→*A3*→A4→A5→A7→A9→A12→A11→A8→A6→* A10*→*A13*→*A14*→A15*. However, the sub-region marked by the *A4* and *A6* do not connect, the same as *A12* and *A14*. It will cause great problem to ergodic the corresponding sub-regions. In this situation, change the segment point order as *A4→A6* and *A12→A14*.

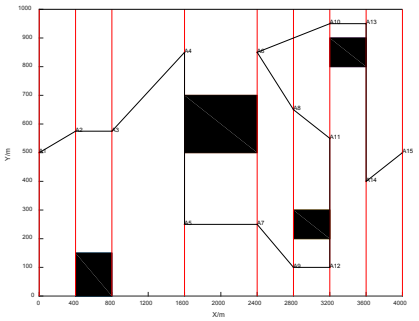

Fig.13 Planning Map by Greedy Algorithm

The Second rule is that in order to avoid the obstacle, the new distance calculation will updated to help determining the point order. The shortest distance of two points is always the only choice. The distance between two points can be calculated as following: Firstly, the distance equals to infinite if there is obstacle between two points, which means the two points is disconnected; secondly, the distance should extra plus the biggest distance of every two connected points.

Distance between every two points can be described by the cost matrix A. $f(A)$ is the cost matrix function, which represents the global cost function, Matrix B represents the additional cost matrix, d_{ij} represents the distance between two points, i and j indicate the current point and the next point, respectively.

$$f(A) = f(A) + B \tag{13}$$

$$A = f(A) \tag{14}$$

$$B = (b_{ij})_{nxn} \tag{15}$$

s.t.

$$f(A)_0 = A_0 = (a_{ij})_{nxn} \tag{16}$$

$$a_{ij} = \begin{cases} 0, & i, j \text{ is connected } \& \ i \equiv j \\ d_{ij}, & i, j \text{ is connected } \& \ i \neq j \\ \infty, & i, j \text{ is not connected} \end{cases} \tag{17}$$

$$b_{ij} = \begin{cases} 0 & , \quad j \text{ is not traversed} \\ \max[(a_{ij}) \mid a_{ij} \neq \infty]_{nxn}, & j \text{ is traversed} \end{cases} \tag{18}$$

The next point can be obtained by the equations. The initial state of the cost matrix is：

$$f(A)_0 = A_0 = (a_{ij})_{nxn} \tag{19}$$

Where a_{ij} indicates the distance between point i and point j. every two points are regarded as disconnected when the straight line connecting the two points passes through the center of the obstacle, the make $a_{ij} = \infty$. Simultaneously, the additional cost Matrix B is updated in the ergodic process in real time.

C. Ergodic Order determination of Boundary Points

The cost matrix is using greedy strategy to determine the path point order of the haze sub-regions. The cost matrix is initialized at the starting point, then automatically updated when an expected point is reached.

After establishing a two-dimensional map, dividing the sub-regions, picking up the boundary point of the point, and setting up the cost matrix, an improved greedy algorithm is adopted to plan the ergodic sequences of the haze sub-regions. As shown in Figure 14, the initial point is *A*1. The initial cost matrix can be determined by the distance between the every two points. If there is an obstacle between the two points, the distance between them is infinite. The object of the greedy algorithm is finding an point which has the minimum distance between the current point. The next point connected to *A1* is determined to be *A2*. Then taken *A2* as the current point, becomes, updating the global cost matrix, and the next point connected to *A2* is determined to be *A3*. Finally, the points traversal sequence can be determined as shown in Figure 14.

*A*1→*A*2→*A*3→*A*4→*A*6→*A*8→*A*11→*A*14→*A*15→*A*13→*A*10→*A*12→*A*9→*A*7→*A*5。

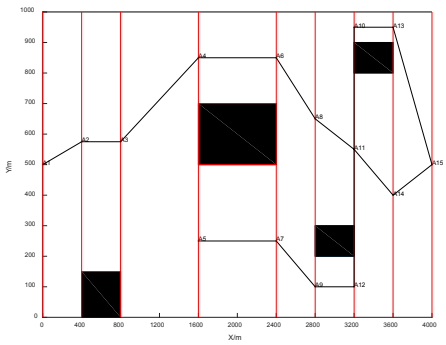

Fig.14 Haze area traversal sequence diagram

IV. SIMULATION AND RESULT ANALYSIS OF HAZE REMOVAL ALGORITHM

A. Ergodic Algorithm Selection

After determining the traversal order of the haze sub-area, the key problem left is how to planning the path of the Soft-Wing UAV to complete the coverage of the haze sub-regions. In order to improve efficiency, reduce blindness, non-random path planning algorithm is selected. The path planning algorithms conclude reentrant algorithm and spiral algorithm. Considering the dynamic constraints of the Soft-Wing UAV, the spiral algorithm may cause the Soft-Wing UAV to stall due to a small turning radius, and it will cause the Soft-Wing UAV having deteriorate performance and falling down directly. Therefore, foldback algorithm is adopted to traverse haze sub-regions.

B. Ergodic Simulation

The haze sub-regions are traversed using the foldback algorithm. If the sub-region is fully traversed, it will move to the next location according to the planned path. Combining the ergodic algorithm with Soft-Wing UAV controller, the haze removal results are shown in Fig.15. The red line indicates the expected haze removal trajectory, the blue line indicates the actual haze removal trajectory.

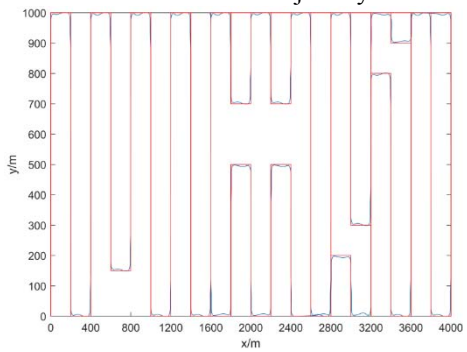

Fig.15. Ergodic effect diagram of Soft-Wing UAV

C. Evaluation Index

50 pair points of the real-time position and the expected position are selected randomly in the haze removal simulation of Soft-Wing UAV, which is taken as the reference point and actual point of the evaluation index in the process of straight-line and turning. The expected point position is (X_i, Y_i) and

the actual point position is (X_i', Y_i').

Firstly, let

$$A_i = (X_i^2 + Y_i^2)^{1/2} \tag{20}$$

Then, make standardize operations:

$$A_i^* = \frac{A_i - E(A_i)}{[\mathrm{var}(A_i)]^{1/2}} \tag{21}$$

Finally, calculate the relative deviation:

$$\Delta_i = \frac{[(X_i - X_i')^2 + (Y_i - Y_i')^2]^{1/2}}{A_i^*} * 100\% \tag{22}$$

The smaller the ΔI is, the better the actual trajectory fits the desired trajectory of haze removal. If $\Delta_i = 0$, the actual trajectory of haze removal completely fits the desired trajectory of haze removal. Therefore, the value of Δ_i can reflects the operation effect well or not.

After calculating with the above formula, the simulation results show that the actual deviation between the actual trajectory of haze removal and the expected trajectory of haze removal is less than 0.5%. Therefore, the Soft-Wing UAV ergodic planning algorithm can make a good haze removal.

V. CONCLUSION

In this paper, a five-channel Soft-Wing UAV transfer function model is used to build a SIMULINK simulation platform. Numerical simulations verified the accuracy with autonomous control of forward speed, vertical velocity, and yaw velocity. Two track control strategies with track flight simulations are realized for straight line and turn operations. An ergodic plan algorithm based on the improved greedy algorithm combined with foldback algorithm is proposed. Finally, the model of haze area is simulated, and numerical simulation is carried out to testify the effectiveness of the proposed algorithm. The deviation of the actual haze removal trajectory from the expected haze removal trajectory is less than 0.5%, which verifies the reliability of the haze removal algorithm for Soft-Wing UAV.

REFERENCES

[1] LiMin Zhou, Yunuo Ma. “"Public-Private Partnership", Environmental Pollution and Governance of Haze Disasters,”*Risk Disaster Crisis Research*, 2017, pp. 31-45.

[2] WHO report. “First identification of air pollutants carcinogenic,” *Chinese Journal of Food*, 2013, pp. 114-115.

[3] MingYuan Liu, JiaXin Pang. “Analysis of the Present Situation of Air Pollution in China and Its Legal Countermeasures from the Phenomenon of Haze,” *Legal System & Society*, 2016, pp. 174-175.

[4] “There are big tricks to deal with fog,” *Invention & Innovation*, 2016, pp. 9-10.

[5] Yu Chen, Ying Zeng, ZhiPeng Luo. “New heating and cooling fog and smart helmet,”*Technology Innovation & Application*, 2017, pp. 9-10.

[6] XianYu Meng, WenXin Ma, HuaLun Dong, Zan Wang. “Research and Application of Electrostatic Haze Removal Technology,” *Modern Salt Chemicals*, 2017, pp. 49-50.

[7] Zhenshi Zhang, Huanle Pei, Huangke Chen, Yipeng Li. “A Quantitative Mechanism Based on Environmental Compensation for Trash Incineration,” *International Conference on Modelling, Identification and Control*, 2015, pp. 252-256.

[8] Carlos Ocampo Martinez, Zakaria Baroud, Atallah Benalia. “Robust fuzzy sliding mode control for air supply on PEM fuel cell system,” *International Journal of Modelling Identification & Control*, 2018, 29(4), pp. 341.

[9] JunTong Qi, Liying Yang. “Self-developed Fly-wing UAV Autonomous Flight Control and Simulation Research,” *Journal of System Simulation*, 2015, pp. 2988-2997.

[10] JinDa Liu. “Soft-wing UAV autonomous flight control and visual simulation,” *Northeastern University*, 2014.

[11] Slegers N, Costello M. “Aspects of Control for Parafoil and Payload System,” *Journal of Guidance, Control & Dynamics*, 2015, pp. 898-905.

[12] Chrystine M. “Modeling of Parafoil-Payload Relative Yawing Motion on Autonomous Parafoils,” *AIAA Aerodynamic Decelerator Systems Technology Conference and Seminar*, 2011, pp. 23-26.

[13] Gibong H. “Identification of Powered Parafoil-Vehicle Dynamics from Modelling and Flight Test Data,” *Texas: Texas A&M University*, 2005.

[14] JunTao Zhang, ZhongXi Hou. “Longitudinal Dynamic Modeling of Power Wing Umbrella System,” *Journal of System Simulation*, 2010, pp. 2541-2545.

[15] Nathan J. Slegers. “Effects of Canopy-Payload Relative Motion on Control of Autonomous Parafoils,” *Journal of Guidance, Control & Dynamics*, 2015, pp.116-125.

[16] Michael Ward. “Evaluation of Multi-body Parafoil Dynamics Using Distributed Miniature Wireless Sensors,” *AIAA Atmospheric Flight Mechanics Conference*, 2011.

[17] Mooij.E, Wijnands.Q. Schat.B. “9 doF Parafoil/Payload Simulator Development and Validation,” *Aiaa Modeling & Simulation Technologies Conference*, Austin, 2003.

[18] Slegers.NJ. “Effects of Canopy-Payload Relative Motion on Control of Autonomous Parafoils,” *Journal of Guidance, Control & Dynamics*, 2015, pp. 116-125.

[19] S Masroor, DB Wang, M Aamir, ZA Ali. “MRAC base robust RST control scheme for the application of UAV,” *International Journal of Modelling Identification & Control*, 2017, 28(3), pp. 232.

[20] W Jasim, D Gu. “Robust path tracking control for quadrotors with experimental validation,” *International Journal of Modelling Identification & Control*, 2018, 29(1), pp. 1.

[21] F Zhou, W Zhang, Z Wang. “Real-time Motion Estimation for UAVs Based on Dissimilar Multi-sensor Data Fusion,” *Jiqiren/robot*, 2015, 37(1), pp. 94-101.

[22] C Peng, Y Bai, G Qiao, X Gong, Y Tian. “Anti-windup and Multi-Mode PID Control of Yaw Movement for a Quad-Rotor UAV,” *Robot*, 2015, 37(4), pp. 415-423.

[23] BingBing Li, Fan Liu, JunTong Qi, Sen Mei, TianYu Lin, JianDa Han. “Soft-Wing UAV flight test and transfer function model identification, Thirty-fourth,” *China Control Association*, 2015. pp. 430-436.